Effect of milling mechanism on the CO_2 capture performance of limestone in the Calcium Looping process

Monica Benitez-Guerrero, [a, b] Jose Manuel Valverde,[a *] Antonio Perejon, [b, c] Pedro E. Sanchez-Jimenez [b] and Luis A. Perez-Maqueda [b]

[a] Facultad de Física, Universidad de Sevilla, Avenida Reina Mercedes s/n, 41012 Sevilla, Spain.

[b] Instituto de Ciencia de Materiales de Sevilla, C.S.I.C.-Universidad de Sevilla, C. Américo Vespucio nº49, 41092 Sevilla, Spain.

[c] Facultad de Química, Universidad de Sevilla, Avenida Reina Mercedes s/n, 41012 Sevilla Spain.

*Prof. Dr. J.M. Valverde
Facultad de Física
Universidad de Sevilla
Avenida Reina Mercedes s/n, 41012 Sevilla (Spain)
Tel +34 954550960 Fax +34 954239434
E-mail: jmillan@us.es

Effect of milling mechanism on the CO_2 capture performance of limestone in the Calcium Looping process

Highlights:

* Limestone samples were subjected to mechanical milling using diverse mills based on different mechanisms

* The multicycle Calcium Looping performance of the samples depends critically on the milling mechanism

* Shear and impact based dry-millings promote sintering of the nascent CaO after calcination, which hinders CO_2 capture

* In contrast, highly energetic dry-milling combining impact and shear forces (EMAX) promotes CO_2 capture

* CaO porosity and solid-state diffusion of CO_2 during carbonation are enhanced by EMAX ball mill

Abstract:

This work analyzes the relevant influence of milling on the CO_2 capture performance of natural limestone. Diverse types of milling mechanisms produce contrasting effects on the microstructure of the CaO formed after calcination of the milled samples, which affects crucially the kinetics of carbonation at conditions for CO_2 capture. The capture capacity of limestone samples milled using either shear or impact based mills is impaired compared to as-received limestone. After calcination of the milled samples, the resulting CaO porosity is increased while crystallinity is enhanced, which hinders carbonation. Conversely, if the material is simultaneously subjected to intense impact and shear stresses, CaO porosity is promoted whereas CaO cristanillity is reduced, which enhances carbonation in both the reaction and solid-state diffusion controlled regimes.

Keywords: Ball milling • Calcium-Looping • CO_2 capture • Crystallite size • Porosity

1. Introduction

The 21th conference on global warming (COP21) was ended with a commitment to limit the increase of the global average temperature to 2.0 ^{o}C in 2100 [1]. Such a great challenge would be feasible by promoting the share of renewable energies, a rational use of fossil fuels and the use of carbon capture technologies to reduce the emissions of CO_2 in power plants. In this regard, the Calcium Looping (CaL) process has lastly received considerable interest as a potentially cheap, environmentally friendly and efficient CO_2 capture technology at the necessarily large scale that involves retrofitting commercial fossil fuel fired power plants [2] [3] [4] [5].

The CaL process for CO_2 capture, which has been already demonstrated at large pilot scale (1-2 MW_{th}) [6] [7] [8] [9], is based on the reversible carbonation/calcination reaction of CaO:

$$CaO_{(s)} + CO_{2\,(g)} \rightleftarrows CaCO_{3\,(s)}; \quad \Delta Hr^{0} = -178\ kJ\ mol^{-1} \qquad (1)$$

Thus, the flue gas stream from a combustion plant (carrying a concentration of CO_2 close to 15 vol% in the case of coal) is used to fluidize a bed of CaO particles at atmospheric pressure, where quick carbonation takes place at around 650 ^{o}C. The carbonated particles are transferred to a second fluidized bed reactor where calcination occurs under high CO_2 concentration (above 70 vol%) at temperatures ~930-950 ^{o}C in short residence times, which is achieved by oxy-fuel combustion to avoid CO_2 dilution [6] [10]. Calcination serves to regenerate the CaO particles and produces a concentrated CO_2 gas stream, which is extracted from the calciner, compressed and stored or employed for other uses. A schematic diagram of the process is shown in Figure 1.

Among the different CaO-based materials to be employed in the CaL process, natural limestone (near 100% $CaCO_3$) is a preferred CaO precursor due to its low price (about 10€/ton), abundance and nontoxicity [11] [12]. However, the CaO derived from natural limestone calcination exhibits a progressive decay of its CO_2 capture capacity as the number of carbonation/calcination cycles is increased [13] [14] [15] [16], which makes it necessary to introduce a make-up flow of fresh limestone while the spent sorbent is periodically purged from the system. A drastic reduction of the CaO surface area due to marked sintering in the calcination stage at the harsh conditions of the process is a main limiting mechanism for carbonation as widely reported in the literature [17] [18] [19].

Many different strategies to mitigate CaO sintering have been pursued in recent works such as the use of thermally stable inert additives [4] [11] [12] and the use of pelletizing methods to maintain a porous structure [20] [21] [22]. An alternative simple and cost-effective method to produce porous Ca-based sorbents scalable to the industrial level is mechanical milling. Mechanical milling leads to a reduction of $CaCO_3$ crystallinity, thus favoring the kinetics of calcination, which reduces the temperature needed to achieve full calcination in short residence times [23] [24] . Nevertheless, the literature on the effect of milling on the performance of CaO-based materials for CO_2 capture is yet scarce [23] [25] [26]. The use of different types of CaO precursors (limestone, dolomite, etc.) [23] [26], calcination conditions (mild or harsh as would be the case for CO_2 capture) [25] [24] [26], and milling media (dry or wet) [25] [26], lead to diverse results. Some of these works point out to the reduction of particle size as the main cause for the enhancement of CaO activity [25] [26], whereas others highlight the role of milling on CaO crystallinity [23] [24]. On the other hand, milling has been shown to enhance the multicycle CaO activity in [24] whereas the opposite effect is reported elsewhere [23]. This work is focused on getting a grip on the relevant mechanism involved on the CO_2 capture capacity of milled limestone in order to reconciliate these apparently contradictory results. To this end, several mills have been employed, which operate by

applying different types of stress on the sample. As will be seen, the behavior of limestone in the CaL process previously subjected to mechanical milling depends on the type of stress acting on the sample predominant during the milling process, which affects critically the reactivity of the milled solids.

2. Material and methods

High-purity natural limestone from Matagallar quarry (Sevilla, Spain) (99.5% wt $CaCO_3$) was employed in the present work. The as-received limestone was supplied in powder form (particle size < 45 μm) by Segura S.L. Company. Samples were mechanically milled in a very high-energy ball mill EMAX (Retsch), which achieves maximum intensity ball grinding in short times by the joint action of impact and shear stresses. 100 cm^3 steel jars and 50 steel balls per jar with a diameter of 10 mm were employed for milling. The limestone sample weight to ball ratio was set to 1:20 and the sample mass in each jar was 10 g. The limestone sample was milled at 1500 rpm for 90 s under dry air. This short milling time was selected attending to the results on the evolution of $CaCO_3$ crystallite size with the milling time (Figure 2). As can be seen in Fig. 2, for the EMAX mill the coherent crystal length (crystallite size) reaches a minimum value after just about 90 s milling. This milling time is much smaller as compared with the time required by the other different milling procedures employed in the present work as briefly described below. Crystallite size of the milled samples was estimated using the Scherrer equation applied to the maximum intensity (104) Bragg reflection peak.

For the sake of comparison, results obtained in a recently published work [23], where samples were grinded in other mills, are used in the present manuscript. In that work, a centrifugal ball mill (Fritsch Pulverisette) was employed, which subjects the sample to mainly shear stresses. Besides, a SPEX 8000 ball mill was also employed, which creates high energy

impact forces on the limestone particles. Further details on the milling conditions in these mills can be seen in [23] .

Particle size distributions (PSDs) were analyzed by laser granulometry, using a Mastersizer 2000 (Malvern). For this purpose, samples were previously dispersed in 2-propanol and sonicated for 30 s to loose particle agglomerates.

Measurements on the multicycle CaO conversion were performed using a Q5000IR thermogravimetric analyzer (TA instrument), equipped with a high sensitive balance (< 0.1 μg) and a furnace heated by IR halogen lamps, which allows achieving very high heating and cooling rates (up to 300 ^{o}C/min) as well as stable isotherms. Each experiment was started by a calcination step from room temperature to 900 ^{o}C (at 300 ^{o}C/min, and held for 5 min) under high CO_2 concentration (70% CO_2/ 30% air vol/vol) at atmospheric pressure. The milled samples exhibited full calcination at this relatively reduced temperature (900 ^{o}C) as compared with as-received limestone (> 930 ^{o}C) [23]. The precalcination stage was followed by a carbonation stage quickly decreasing the temperature to 650 ^{o}C at 300 ^{o}C/min, which was held for 5 min under 15% CO_2/ 85% air vol/vol. As discussed in detail in previous works, achieving quick transitions between both stages is of paramount importance to mimic realistic CaL conditions for CO_2 capture necessarily involving high CO_2 concentration in the calcination stage [27]. A total of 20 carbonation/calcination cycles were run in which a fixed and small mass (10 mg) was used for avoiding undesired effects due to CO_2 diffusion resistance across the sample bulk. The scheme of the procedure is shown in Figure A1 (Appendix), where the temperature curves recorded for the program and sample are compared. As can be seen, there is a quite good match in the ramps and a high temperature accuracy at the isotherms, which complies with the specifications provided by the manufacturer (+/- 1 ^{o}C).

In the practical application the method employed in industry to calcine under a rich CO_2 atmosphere in order to avoid CO_2 dilution is oxy-combustion. Oxy-combustion leads to the

generation also of H_2O, which gives rise to a CO_2 concentration in the calciner between 70 and 90% v/v. The thermogravimetric apparatus employed in our study does not allow for the introduction of H_2O due to its corrosiveness, thus we chose to use 70%CO_2/30%air atmosphere to replicate the CO_2 concentration in the calciner. Expectedly, the presence of H_2O would accelerate the reaction as reported in previous works [28].

In addition to TGA tests, calcination of the samples was performed in a separate tubular furnace to obtain sufficient mass for physisorption analysis. In this furnace, a 1 gram sample was subjected to calcination under CO_2 for 90 min at 900 ^oC. CO_2 was displaced by N_2 at 850 ^oC during cooling to avoid recarbonation. These tests served to investigate the effect of the type of milling mechanism on the porosity of the CaO generated after calcination in a high CO_2 concentration environment.

Nitrogen physisorption analysis at -196 ^oC was performed using an ASAP2420 (Micromeritics) instrument. Prior to the analysis, the samples were degassed at 350 ^oC for 8 h. BET Surface area (S_{BET}) was calculated according to the BET equation [29]. Pore volume (V_{sp}) was determined from the amount of nitrogen adsorbed at a P/P_0 value of 0.99. The mesopore size distributions were determined applying the Barett-Joyner-Halenda (BJH) method to the desorption branch of the isotherms [30], and the average pore sizes (Wp and Wp_{BJH}) were calculated by approximating the pore geometry to a cylinder.

In-situ thermo X-ray diffraction (TXRD) measurements during calcination under CO_2 were carried out using a D8 Advance diffractometer (Bruker), equipped with a XRX 900 high temperature chamber (Anton Paar) and a high sensitivity and fast response detector (Vantec 1, Bruker). To this end, the samples were heated from ambient temperature to 925 ^oC at a rate of 10 °C/min under CO_2. XRD scans were recorded at 25 ^oC intervals in the range 2θ = 20 - 60° for 295 s and using a 0.03° step. Once the target calcination temperature was reached, it was maintained for 60 min while XRD scans were continuously recorded. Instrumental contribution

for structural adjustments was assessed in a wide range of diffraction angles using LaB_6 and silicon standards. The crystallite sizes of $CaCO_3$ and CaO during in-situ calcination were calculated by means of the Le Bail quantitative method [31].

Scanning electron micrographs of previously gold-sputtered (2 min, 20 mA in an Emitech K550 Telstar sputter-coating) samples were acquired using a Hitachi S4800 SEM-FEG microscope.

3. Results and Discussion

Milling of the as-received limestone, as described in previous section, yielded an increase of particle size (seen in SEM micrographs of Figure 3 and particle size distribution data in Figure 4). Arguably, particles are enlarged during milling by cold welding as widely reported in the specialized literature [32] [33], which is promoted for low hardness solids such as calcite (3 on the Mohs scale). The diverse milling mechanisms acting in the EMAX, SPEX and Fritsch mills do not have a relevant effect on the particle size distribution of the milled samples. Similar bimodal distributions just slightly shifted were obtained (Figure 4). High energy milling, as performed in the EMAX and SPEX mills, leads to a median particle size ($D_{v(50)}$) which is about 6 times larger the median particle size of the as-received limestone. On the other hand, the relatively lower energy centrifugal milling (Fritsch mill) produces a smaller $D_{v(50)}$ value, which was only around 2.5 times the as-received limestone median particle size.

Structural parameters of milled limestone samples such as surface area S_{BET} and pore volume V_{sp} are shown in Table 1. As may be seen, the S_{BET} and V_{sp} values of limestone after being milled are almost twice and three times the corresponding values for the as-received limestone. The increment of the median particle size and the increase of surface area and

porosity for the milled limestone samples can be explained by the formation of agglomerates with new cavities and inner pores accessible to nitrogen. Therefore, these results are related to the increase of the population of pores in the mesoporous range (5-50 nm) due to a modification of particle morphology, which is consistent with the reduction of the coherent crystalline domain of $CaCO_3$ (crystallite size ~20 nm), shown in Figure 2 .

Table 1 also shows surface area and porosity data of the samples calcined in tubular oven under pure CO_2 atmosphere. After calcination and loss of CO_2, new pores are generated and the surface area values raise, as observed for the raw and milled limestones, being the effect more relevant for EMAX milling. This growth is almost inappreciable for the calcined Fritsch milled sample, which exhibits a surface area lower than the calcined limestone. This result can be explained due to its different micro and nanostructure, which could collapse under the harsh calcination conditions employed.

Table 1: Porosimetry measured data for as-received and milled limestone samples and for the calcined products (CaO) in a CO_2 atmosphere.

	Limestone	**Fritsch Mill**	**SPEX Mill**	**EMAX Mill**
$CaCO_3$ samples				
S_{BET} (m^2/g)	2.8	5.1	3.6	5.5
V_{sp} (cm^3/g)	0.006	0.016	0.013	0.019
W_p (nm) [a]	9.1	12.3	14.0	14.2
$W_{p\,BJH}$ (nm) [b]	19.2	19.6	19.8	18.2
CaO samples [c]				
S_{BET} (m^2/g)	10.2	5.9	13.7	18.7
V_{sp} (cm^3/g)	0.037	0.018	0.034	0.064
W_p (nm) [a]	14.7	12.4	9.8	13.6
$W_{p\,BJH}$ (nm) [b]	34.8	35.7	30.6	33.3

a Mean pore width, Wp = 4V/S

b Mean BJH pore width, determined by BJH desorption branch data (4V/S)

c CaO samples after a calcination in CO_2

Examples of the time evolution of carbonation are illustrated in Figure 5, which shows the time evolution of sample weight for the as-received and milled limestone samples measured by thermogravimetric analysis (TGA) during the N=2, 5, and 20 carbonation/calcination cycles. As previously reported in the literature, it may be seen that the carbonation stage takes place through two well differentiated phases [15] [34]. Firstly, carbonation occurs through a short fast reaction controlled phase (FRP) that takes place on the free surface of the CaO particles. This fast phase is followed by a relatively slower phase, where carbonation is governed by the counter-current solid-state diffusion of CO_3^{2-} and O^{2-} anions across the $CaCO_3$ product layer built upon the CaO surface in the fast regime [35] [36]. As described in previous works [24] [37] [38], the contribution to the overall CO_2 capture of this solid-state diffusion phase (SDP) plays a relevant role on the efficiency and energy consumption for CO_2 capture as depending on the solids residence time in the carbonator. Thus, the enhancement of CO_2 capture in the SDP, as would be the case for example when using dolomite instead of limestone, would help decreasing the energy consumption for CO_2 avoided (SPECCA) while the capture efficiency is kept high [39]. Figure 5 shows that the EMAX milled limestone exhibits a markedly enhanced CO_2 uptake in both the FRP and SDP as compared to as-received limestone. In contrast, carbonation is hindered, especially in the SDP, for the samples milled in the SPEX and Fritsch mills.

The multicycle CaO conversion X_N is the parameter used to evaluate the performances in tests, which is defined as the ratio of the CaO mass converted to $CaCO_3$ in the carbonation stage of the Nth-cycle to the CaO mass before carbonation:

$$X_N = \frac{m_{Carb\,N} - m_N}{m_N} \cdot \frac{56}{44} \quad (2)$$

where m_N and $m_{Carb\ N}$ are the sample masses measured before and after carbonation at the Nth-cycle and 56/44 is the CaO to CO_2 molar masses ratio. Multicycle CaO conversion data for the samples obtained from the diverse millings (EMAX, SPEX and Fritsch mills) and for as-received limestone are shown in Figure 6a. The contributions to the overall conversion in the FRP ($X_{N\,FRC}$) and SDP ($X_{N\,SDC}$) are plotted in Figures 6b and 6c, respectively. The progressive drop of conversion with the number of cycles can be rather well fitted by the semi-empirical equation [16] [40] [41]:

$$X_N = X_r + \frac{X_1}{k(N-1)+(1-X_r/X_1)^{-1}} \quad (3)$$

where N is the cycle number, k is the deactivation rate constant, X_1 is CaO conversion in the first cycle and X_r is the residual conversion after a very large number of cycles. Best fitting curves are shown in Figure 6. Best fitting parameters (k and X_r) are given in Table 2.

Table 2. Best fitting parameters in Eq. 3 (residual conversion and deactivation rate) to overall multicycle CaO conversion $X_{N\ T}$, conversion in the reaction controlled phase $X_{N\ FRP}$ and conversion in the solid-state diffusion controlled phase $X_{N\ SDP}$ (Figure 6). Standard errors from the regression analysis are included in brackets.

		Limestone	SPEX Mill	Fritsch Mill	EMAX Mill
	k_T	0.549 (±0.013)	0.521 (±0.025)	0.228 (±0.006)	0.427 (±0.008)

$X_{N\ T}$	$X_{r\ T}$	0.077 (±0.001)	0.072 (±0.002)	0.044 (±0.001)	0.093 (±0.001)
	R^2	0.999	0.996	0.999	0.999
	χ^2	1.971E-6	6.538E-6	8.085e-7	1.873E-6
$X_{N\ FRP}$	k_{FRP}	0.375 (±0.020)	0.485 (±0.028)	0.195 (±0.013)	0.467 (±0.019)
	$X_{r\ FRP}$	0.023 (±0.001)	0.037 (±0.001)	0.021 (±0.001)	0.040 (±0.001)
	R^2	0.996	0.9948	0.996	0.998
	χ^2	2.713E-6	2.182E-6	1.000E-6	1.552E-6
$X_{N\ SDP}$	k_{DSP}	0.854 (±0.048)	0.538 (±0.030)	0.419 (±0.025)	0.311 (±0.019)
	$X_{r\ DSP}$	0.053 (±0.001)	0.034 (±0.001)	0.028 (±0.001)	0.044 (±0.002)
	R^2	0.995	0.995	0.994	0.994
	χ^2	2.035E-6	2.631E-6	1.446E-6	1.281E-5

As seen in Figure 6, the EMAX milled limestone shows the highest CaO conversion both in the FRP and the SDP. The enhancement of conversion is especially relevant in the SDP, which contrasts with the adverse effect caused by the Fritsch and SPEX mills as Figure 5 and 6 reveal. Such opposed effects indicate that the milling mechanism influences strongly the structural properties of the solid, which has relevant consequences on the derived CaO reactivity upon carbonation. Thus, the combination of intense shear and impact stresses acting in the EMAX mill promotes CO_2 capture whereas the individual action of either of these mechanisms alone (impact stresses in the SPEX mill and shear stresses in the Fritsch mill) yield an adverse effect on the CaO reactivity, which is particularly detrimental on carbonation in the SDP. It must be remarked that the aim of this study is just to show the relative drop of conversion in both phases as the number of cycles is increased in order to have a better understanding on how milling affects CO_2 capture in both phases. A rigorous kinetic study of carbonation is out of the scope of our work.

To better understand the underlying causes of these conflicting results, we have analyzed in detail the structure of the CaO resulting from limestone calcination under CO_2 as affected by the milling mechanism. As seen above, the CaO derived from the limestone sample previously milled in the EMAX mill presents a surface area significantly larger than the as-received limestone (Table 1). This result is upheld by the higher porosity observed in the SEM images (Figure 7) and is also demonstrated by the pore size distributions (Figure 8).

The CaO porosity enhancement is consistent with the improved CaO conversion measured for the EMAX milled sample in the FRP (Figure 6b), which is directly proportional to the CaO specific surface area as shown in previous works [16] [34] [40] [42] [43]. As seen from the SEM pictures (Figure 9) of the cycled samples, the cycled CaO from the EMAX milled limestone retains a greater porosity compared to the as-received limestone, which explains the noticeable sustained improvement of CaO conversion as the number of cycles is increased. However, some researches [44] point out that the conversion increase observed for milled limestones is not sufficiently justified by the increase of surface area. In the present work, the proportionality between surface area and FRP conversion is not clearfor Fristch and SPEX milled samples as compared to raw limestone. Both milled limestones exhibit similar FRP conversions whilesurface area and porosity values for the initial calcined sorbent are different (Table 1). On the other hand, it is know that the degree of crystallinity of the CaO formed after calcination critically affects carbonation in the SDP [24] [45]. The results of the present paper suggest that CaO crystallite size influences not only the SDP conversion but also the carbonation conversion in the subsequent FRP phase, which is reminiscent of the effect of crystallinity on a purposely introduced recarbonation stage reported in previous works [46].

In-situ thermo X-ray diffraction analysis were performed to investigate the crystallographic transformation of $CaCO_3$ to CaO during calcination under CO_2, as shown in Figure 10 for the EMAX milled limestone, where the evolution with the temperature of the

main diffraction peaks of $CaCO_3$ and CaO can be appreciated. . Figure 11 shows the crystallite size evolution of the $CaCO_3$ and CaO phases for the as-received and milled limestone samples during in-situ calcination under CO_2. Regardless of the type of milling employed, it is seen that the initial crystallite size of the $CaCO_3$ is reduced from ~100 nm down to ~20 nm by the mechanical pretreatment, in good agreement with data reported in Figure 2. As the temperature is increased from ambient to the onset of calcination (around 900 ºC), the $CaCO_3$ crystallite size is progressively increased. The increase rate of crystallite size is higher for the milled samples compared to the as-received limestone as would be expected since ion diffusion would be notably promoted as the density of defects in the solid structure is increased by milling [47]. Aggregation and sintering phenomena are also affected by the CO_2 atmosphere, which promotes grain boundary diffusion [48] [49] [50].As a result, $CaCO_3$ crystallites reach a similar size for the as-received and milled samples just before the onset of calcination (Figure 11). On the other hand, the milling mechanism does have a relevant influence on the size of the nascent CaO crystallites upon calcination (Figure 11). CaO conversion turns to be controlled by lattice diffusion in the SDP phase and is inversely correlated to CaO crystallite size [24]. Thus, the EMAX milled sample shows a nascent CaO crystallite size ~60 nm, which is slightly below the crystallite size of the CaO derived from the as-received limestone. In contrast, the nascent CaO crystallite size is substantially larger for the SPEX or Fritsch milled samples (above 90 nm). These results explain the effect of the type of milling on the carbonation reactivity in the SDP (Figures 5 and 6c). Thus, the EMAX milled limestone exhibits the highest conversion in this regime since a smaller CaO crystallite size favors solid-state diffusion. Conversely, the carbonation rate in the SDP is relatively lower for the SPEX and Fritsch milled samples, which show accordingly the largest CaO crystallite size Thus, it can be inferred that both milling processes (Fritsch and SPEX) hinder lattice diffusion and limit the CO_2 capture capacity as compared to unmilled limestone. In contrast, the formation of highly reactive surface sites by EMAX milling should promote diffusion,

particularly in the SDP carbonation stage, which leads to a higher CaO overall conversion. However, SPEX and Fristch milling procedures lead to higher CaO crystallite sizes, which should favor deactivation and sintering process, speciallyfor the Fritsch milled sample whose surface area is the lowest, which is consistent with its low capture capacity. Therefore, the altogether action of intense shear and impact stresses in the EMAX mill leads to a higher CaO porosity, which enhances reactivity in the FRP, and also to a smaller CaO crystallite size, which promotes carbonation in the SDP. The individual action of any of these stresses alone (as is the case in the SPEX and Fritsch mills) is however detrimental.

4. Conclusions

This work explores the effect of mechanical milling on the performance of natural limestone in the CaL process for CO_2 capture necessarily involving calcination under high CO_2 concentration. TGA results demonstrate that milling has a relevant influence on the multicycle CaO conversion as depending on the type of milling mechanism. Thus, the joint action of intense shear and impact stress (EMAX mill) lead to a notable improvement on CaO conversion both in the fast reaction and solid-state diffusion controlled regimes. As shown by physisorption analysis the latter effect is due to the enhancement of porosity in the CaO derived from the EMAX milled $CaCO_3$, which promotes the CaO surface area available for carbonation, whereas the former effect is explained from the decrease of CaO crystallinity, which enhances solid-state diffusion. Remarkably, the individual action of either shear or impact forces acting alone in other mills (Fritsch and SPEX mills, respectively) yields a markedly adverse effect on CaO conversion, which is especially noticeable in the solid-state diffusion controlled regime. Accordingly, the size of the nascent CaO crystallites obtained from calcination of the Fritsch and SPEX milled samples is relatively large.

Ball milling has been suggested in previous works as a potential technique to enhance the multicycle CaO activity for CO_2 capture. On the other hand, process simulation results indicate

that the rate of conversion in the solid-state diffusion regime at CaL conditions for CO_2 capture play a decisive role on the specific energy consumption for CO_2 avoided. Our work shows that the performance of milled limestone in this process, particularly in the solid-state diffusion controlled regime, depends strongly on the milling mechanism, which would have therefore important implications in the practical application.

Acknowledgements

This work has been supported by the Spanish Government Agency Ministerio de Economia y Competitividad (MINECO-FEDER funds), contracts CTQ2014-52763-C2, CTQ2017-83602-C2 (-1-R and -2-R). AP thanks financial support from VI PPIT-US and VPPI-US for his current contract. We acknowledge the Microscopy and XRD services of the Innovation, Technology and Research Center of the University of Seville (CITIUS) and the characterization services of the Institute of Materials Science of Seville (ICMS).

References

1. Rodes, C.J., *The 2015 Paris Climate Change Conference: COP21.* Science Progress, 2016. **99**(1): p. 97-104.
2. Stanmore, B.R. and P. Gilot, *Review—calcination and carbonation of limestone during thermal cycling for CO_2 sequestration.* Fuel Processing Technology, 2005. **86**(16): p. 1707-1743.
3. Blamey, J., et al., *The calcium looping cycle for large-scale CO2 capture.* Progress in Energy and Combustion Science, 2010. **36**(2): p. 260-279.
4. Erans, M., V. Manovic, and E.J. Anthony, *Calcium looping sorbents for CO_2 capture.* Applied Energy, 2016. **180**: p. 722-742.
5. Perejón, A., et al., *The Calcium-Looping technology for CO2 capture: On the important roles of energy integration and sorbent behavior.* Applied Energy, 2016. **162**: p. 787-807.
6. Arias, B., et al., *Demonstration of steady state CO2 capture in a 1.7 MWth calcium looping pilot.* International Journal of Greenhouse Gas Control, 2013. **18**: p. 237-245.
7. Chang, M.H., et al., *Design and Experimental Investigation of Calcium Looping Process for 3-kWth and 1.9-MWth Facilities.* Chemical Engineering & Technology, 2013. **36**(9): p. 1525-1532.

8. Ströhle, J., et al., *Carbonate looping experiments in a 1 MWth pilot plant and model validation.* Fuel, 2014. **127**: p. 13-22.
9. Hanak, D.P., E.J. Anthony, and V. Manovic, *A review of developments in pilot-plant testing and modelling of calcium looping process for CO2 capture from power generation systems.* Energy & Environmental Science, 2015. **8**(8): p. 2199-2249.
10. Coppola, A., et al., *Fluidized bed calcium looping cycles for CO2 capture under oxy-firing calcination conditions: Part 1. Assessment of six limestones.* Chemical Engineering Journal, 2013. **231**(Supplement C): p. 537-543.
11. Kierzkowska, A.M., R. Pacciani, and C.R. Müller, *CaO-Based CO_2 Sorbents: From Fundamentals to the Development of New, Highly Effective Materials.* ChemSusChem, 2013. **6**(7): p. 1130-1148.
12. Valverde, J.M., *Ca-based synthetic materials with enhanced CO_2 capture efficiency.* Journal of Materials Chemistry A, 2013. **1**(3): p. 447-468.
13. Abanades, J.C. and D. Alvarez, *Conversion limits in the reaction of CO_2 with lime.* Energy and Fuels, 2003. **17**(2): p. 308-315.
14. Grasa, G.S., et al., *Reactivity of highly cycled particles of CaO in a carbonation/calcination loop.* Chemical Engineering Journal, 2008. **137**(3): p. 561-567.
15. Grasa, G., et al., *Application of the Random Pore Model to the Carbonation Cyclic Reaction.* Aiche Journal, 2009. **55**(5): p. 1246-1255.
16. Valverde, J.M., *A model on the CaO multicyclic conversion in the Ca-looping process.* Chemical Engineering Journal, 2013. **228**: p. 1195-1206.
17. Sun, P., et al., *The effect of CaO sintering on cyclic CO_2 capture in energy systems.* AIChE Journal, 2007. **53**(9): p. 2432-2442.
18. Sun, P., C.J. Lim, and J.R. Grace, *Cyclic CO_2 capture by limestone-derived sorbent during prolonged calcination/carbonation cycling.* AIChE Journal, 2008. **54**(6): p. 1668-1677.
19. Manovic, V., et al., *Influence of calcination conditions on carrying capacity of CaO-based sorbent in CO_2 looping cycles.* Fuel, 2009. **88**(10): p. 1893-1900.
20. Ridha, F.N., et al., *Pelletized CaO-based sorbents treated with organic acids for enhanced CO_2 capture in Ca-looping cycles.* International Journal of Greenhouse Gas Control, 2013. **17**: p. 357-365.
21. Hu, Y., et al., *One-step synthesis of highly efficient CaO-based CO_2 sorbent pellets via gel-casting technique.* Fuel Processing Technology, 2017. **160**: p. 70-77.
22. Xu, Y., et al., *Effect of lignin, cellulose and hemicellulose on calcium looping behavior of CaO-based sorbents derived from extrusion-spherization method.* Chemical Engineering Journal, 2018. **334**: p. 2520-2529.
23. Sanchez-Jimenez, P.E., et al., *Influence of ball milling on CaO crystal growth during limestone and dolomite calcination: Effect on CO_2 capture at Calcium Looping conditions.* Crystal Growth & Design, 2016. **16**: p. 7025-7036.
24. Valverde, J.M., P.E. Sanchez-Jimenez, and L.A. Perez-Maqueda, *Relevant Influence of Limestone Crystallinity on CO_2 Capture in The Ca-Looping Technology at Realistic Calcination Conditions.* Environmental Science & Technology, 2014. **48**(16): p. 9882-9889.
25. Sayyah, M., et al., *Mechanical Activation of CaO-Based Adsorbents for CO_2 Capture.* ChemSusChem, 2013. **6**(1): p. 193-198.
26. Kurlov, A., et al., *Mechanochemically Activated, Calcium Oxide-Based, Magnesium Oxide-Stabilized Carbon Dioxide Sorbents.* ChemSusChem, 2016. **9**(17): p. 2380-2390.
27. Valverde, J.M., P.E. Sanchez-Jimenez, and L.A. Perez-Maqueda, *Ca-looping for postcombustion CO2 capture: A comparative analysis on the performances of dolomite and limestone.* Applied Energy, 2015. **138**: p. 202-215.
28. Valverde, J.M. and S. Medina, *Limestone calcination under calcium-looping conditions for CO2 capture and thermochemical energy storage in the presence of H2O: an in situ XRD analysis.* Physical Chemistry Chemical Physics, 2017. **19**(11): p. 7587-7596.

29. Brunauer, S., P.H. Emmett, and E. Teller, *Adsorption of Gases in Multimolecular Layers.* Journal of the American Chemical Society, 1938. **60**(2): p. 309-319.
30. Barrett, E.P., L.G. Joyner, and P.P. Halenda, *The Determination of Pore Volume and Area Distributions in Porous Substances. I. Computations from Nitrogen Isotherms.* Journal of the American Chemical Society, 1951. **73**(1): p. 373-380.
31. Le Bail, A., *Whole powder pattern decomposition methods and applications: A retrospection.* Powder Diffraction, 2005. **20**(4): p. 316-326.
32. Choi, H., W. Lee, and S. Kim, *Effect of grinding aids on the kinetics of fine grinding energy consumed of calcite powders by a stirred ball mill.* Advanced Powder Technology, 2009. **20**(4): p. 350-354.
33. Sayyah, M., *Calcium Oxide-Based Sorbents for CO_2 Capture at High Temperature*, in *Chemical and Biomolecular Engr*. 2013, University of Illinois at Urbana-Champaign: United States -- Illinois. p. 143.
34. Barker, R., *The reversibility of the reaction $CaCO_3 \rightleftarrows CaO+CO_2$.* Journal of Applied Chemistry and Biotechnology, 1973. **23**(10): p. 733-742.
35. Bhatia, S.K. and D.D. Perlmutter, *Effect of the product layer on the kinetics of the CO_2-lime reaction.* AIChE Journal, 1983. **29**(1): p. 79-86.
36. Sun, Z., et al., *Ionic diffusion through Calcite (CaCO3) layer during the reaction of CaO and CO2.* Chemical Engineering Science, 2012. **81**: p. 164-168.
37. Ortiz, C., et al., *The Oxy-CaL process: A novel CO_2 capture system by integrating partial oxy-combustion with the Calcium-Looping process.* Applied Energy, 2017. **196**: p. 1-17.
38. Benitez-Guerrero, M., et al., *Large-scale high-temperature solar energy storage using natural minerals.* Solar Energy Materials and Solar Cells, 2017. **168**: p. 14-21.
39. Ortiz, C., J.M. Valverde, and R. Chacartegui, *Energy Consumption for CO2 Capture by means of the Calcium Looping Process: A Comparative Analysis using Limestone, Dolomite, and Steel Slag.* Energy Technology, 2016. **4**(10): p. 1317-1327.
40. Grasa, G.S. and J.C. Abanades, *CO2 Capture Capacity of CaO in Long Series of Carbonation/Calcination Cycles.* Industrial & Engineering Chemistry Research, 2006. **45**(26): p. 8846-8851.
41. Valverde, J.M., et al., *CO_2 multicyclic capture of pretreated/doped CaO in the Ca-looping process. Theory and experiments.* Physical Chemistry Chemical Physics, 2013. **15**(28): p. 11775-11793.
42. Akgsornpeak, A., et al., *Development of synthetic CaO sorbents via CTAB-assisted sol–gel method for CO_2 capture at high temperature.* Chemical Engineering Journal, 2014. **237**(Supplement C): p. 189-198.
43. Valverde, J.M., P.E. Sanchez-Jimenez, and L.A. Perez-Maqueda, *Limestone calcination nearby equilibrium: Kinetics, CaO crystal structure, sintering and reactivity.* The Journal of Physical Chemistry C, 2015. **119**(4): p. 1623-1641.
44. Manovic, V. and E.J. Anthony, *Parametric Study on the CO2 Capture Capacity of CaO-Based Sorbents in Looping Cycles.* Energy & Fuels, 2008. **22**(3): p. 1851-1857.
45. Valverde, J.M. and S. Medina, *Crystallographic transformation of limestone during calcination under CO_2.* Physical Chemistry Chemical Physics, 2015. **17**(34): p. 21912-21926.
46. Valverde, J.M., et al., *Role of crystal structure on CO_2 capture by limestone derived CaO subjected to carbonation/recarbonation/calcination cycles at Ca-looping conditions.* Applied Energy, 2014. **125**: p. 264-275.
47. Heitjans, P. and S. Indris, *Fast diffusion in nanocrystalline ceramics prepared by ball milling.* Journal of Materials Science, 2004. **39**(16): p. 5091-5096.
48. Borgwardt, R.H., *Calcium oxide sintering in atmospheres containing water and carbon dioxide.* Industrial & Engineering Chemistry Research, 1989. **28**(4): p. 493-500.

49. Butler, J.W., C.J. Lim, and J.R. Grace, *CO_2 capture capacity of CaO in long series of pressure swing sorption cycles.* Chemical Engineering Research and Design, 2011. **89**(9): p. 1794-1804.
50. Valverde, J.M., P.E. Sanchez-Jimenez, and L.A. Perez-Maqueda, *Calcium-looping for post-combustion CO_2 capture. On the adverse effect of sorbent regeneration under CO_2.* Applied Energy, 2014. **126**: p. 161-171.

Figure Captions

Figure 1. Schematic representation of the Ca-Looping process for CO_2 capture.

Figure 2. $CaCO_3$ crystallite size of the limestone milled using different mills (a) and using the EMAX mill (b) as a function of the milling time period.

Figure 3. SEM micrographs of as-received natural limestone (a, b) and of the sample milled in the EMAX mill (c, d). The selected areas clearly shows the agglomeration of larger particles in the milled sample as compared to unmilled limestone, which evidences the cold fusion effect during milling.

Figure 4. Particle size distribution measured for as-received and limestone samples in the different mills. Values of the median particle diameter $D_{v(50)}$ are shown in the inset.

Figure 5. Time evolution of temperature and sample weight during the 2nd, 5th and 20th carbonation/calcination cycles for as-received and milled limestone samples. The fast reaction controlled (I) and the slow solid-state diffusion controlled (II) phases taking place during the 5 min carbonation stage are indicated.

Figure 6. a) Multicycle overall CaO conversion measured at the end of the 5 min carbonation stage; b) Multicycle CaO conversion in the fast reaction controlled phase; c) Multicycle CaO conversion in the slow solid-state diffusion controlled phase. Data are shown for as-received and EMAX, Fritsch, and SPEX milled limestones. The solids lines are the best fits from Eq. (3). Best fitting parameters are shown in Table 2.

Figure 7. SEM micrographs of CaO obtained from as-received (a-c) and EMAX milled (d-f) limestone samples after calcination under CO_2.

Figure 8. BJH pore size distributions of CaO obtained from as-received and milled limestone samples after calcination under CO_2.

Figure 9. SEM micrographs of CaO from as-received (a-c) and EMAX milled (d-f) limestones after 20th carbonation/calcination cycles.

Figure 10. In situ thermo XRD scans for the EMAX milled limestone, where the evolution with the temperature of the main diffraction peaks of $CaCO_3$ and CaO is shown (a) and detail of the first and last scans at 100 and 925 ºC respectively (b).

Figure 11. Time evolution of $CaCO_3$ and CaO crystallite sizes and temperature during calcination under CO_2 of as-received limestone and EMAX, Fritsch, and SPEX milled samples (calculated by the Le Bail method [27] from in-situ XRD measurements).

Figure A1 (Appendix/ Supplementary Material). Program temperature curve carried out to test the CO_2 capture multicycle performance using a Q5000IR thermogravimetric analyzer (TA Instruments), and the corresponding sample temperature curve. The shadowed regions show the CO_2 concentration used in each calcination/carbonation step (a). Detail of the onset of the isotherm at the calcination (b) and carbonation (c) stages.

Figure 1

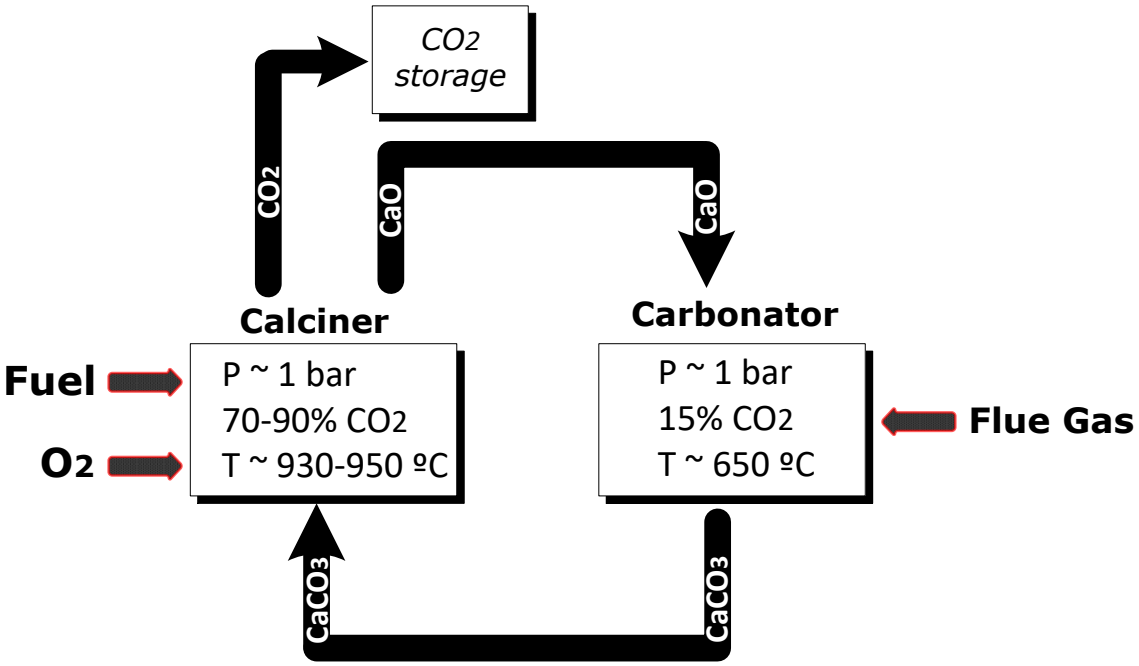
CO2 storage
CO2
CaO
CaO
Calciner
Carbonator
Fuel
O2
P ~ 1 bar
70-90% CO2
T ~ 930-950 ºC
P ~ 1 bar
15% CO2
T ~ 650 ºC
Flue Gas
CaCO3
CaCO3

Figure 2

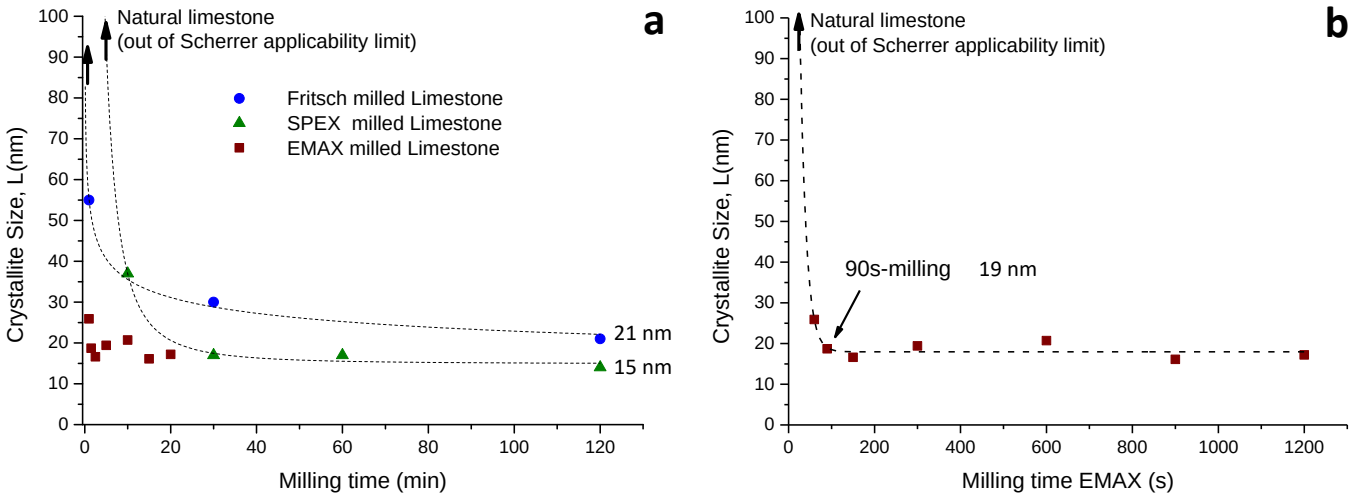
a
Natural limestone
(out of Scherrer applicability limit)
Fritsch milled Limestone
SPEX milled Limestone
EMAX milled Limestone
21 nm
15 nm
Crystallite Size, L(nm)
Milling time (min)
b
Natural limestone
(out of Scherrer applicability limit)
90s-milling
19 nm
Crystallite Size, L(nm)
Milling time EMAX (s)

Figure 3

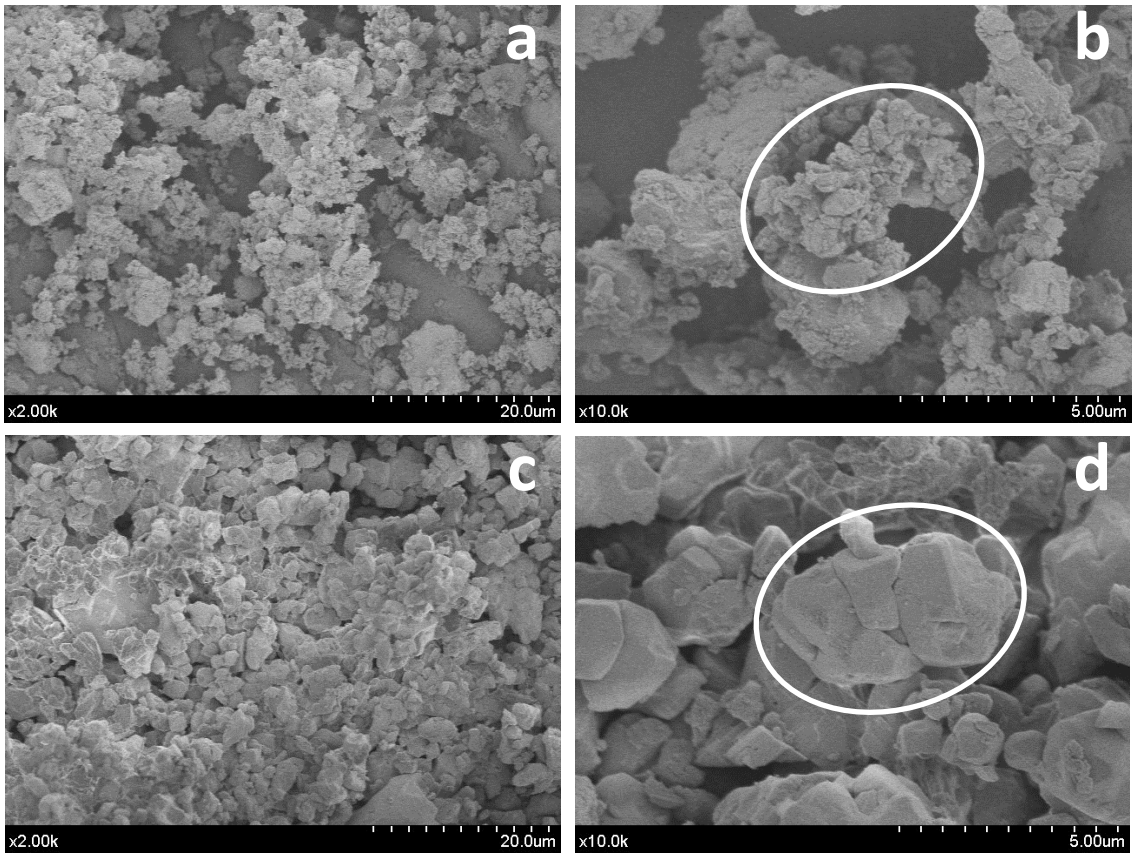

Figure 4

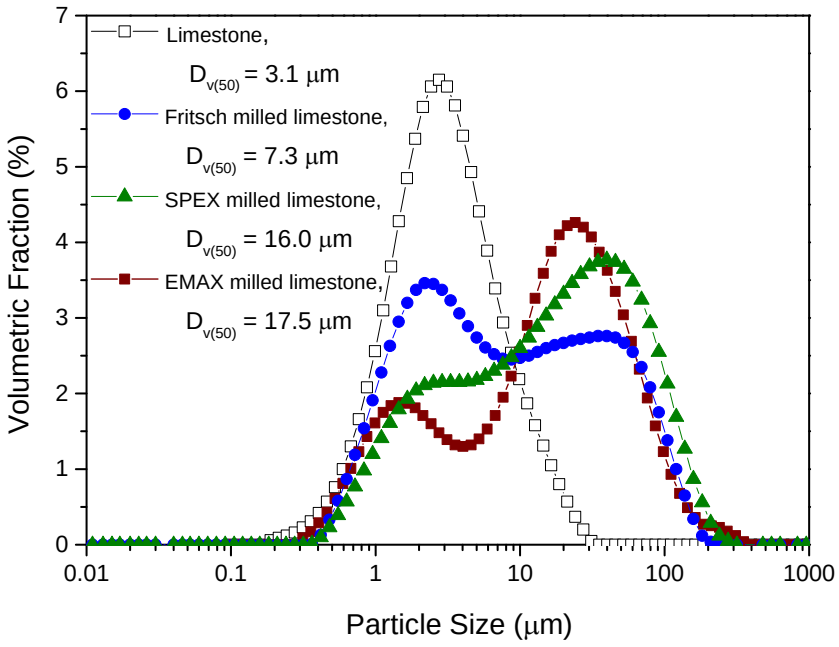
Limestone,
$D_{v(50)}$ = 3.1 μm
Fritsch milled limestone,
$D_{v(50)}$ = 7.3 μm
SPEX milled limestone,
$D_{v(50)}$ = 16.0 μm
EMAX milled limestone,
$D_{v(50)}$ = 17.5 μm
Volumetric Fraction (%)
Particle Size (μm)
0
1
2
3
4
5
6
7
0.01
0.1
1
10
100
1000

Figure 5

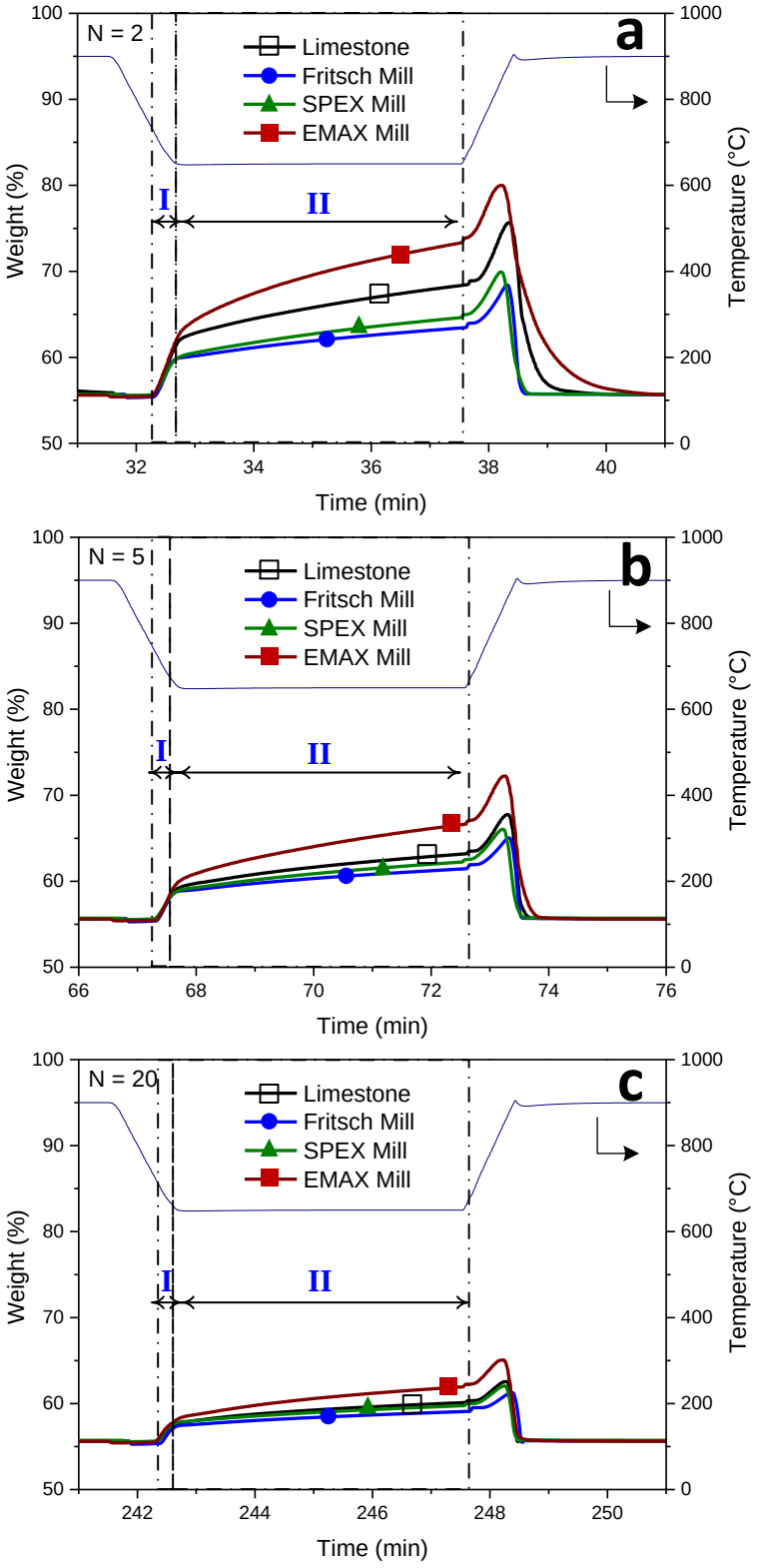
N = 2
a
Limestone
Fritsch Mill
SPEX Mill
EMAX Mill
I
II
Weight (%)
Temperature (°C)
Time (min)
N = 5
b
N = 20
c

Figure 6

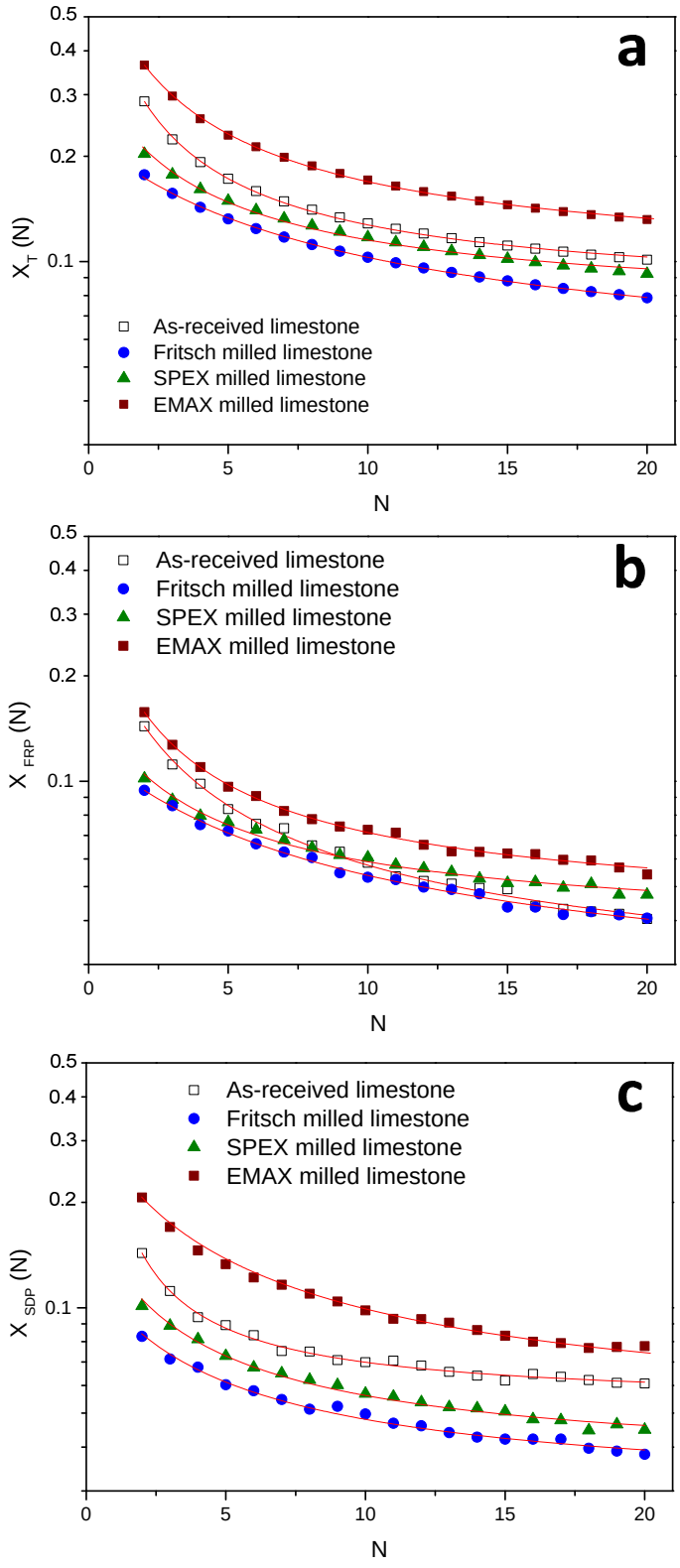
a
X_T (N)
0.5
0.4
0.3
0.2
0.1
0
5
10
15
20
N
As-received limestone
Fritsch milled limestone
SPEX milled limestone
EMAX milled limestone
b
X_{FRP} (N)
c
X_{SDP} (N)

Figure 7

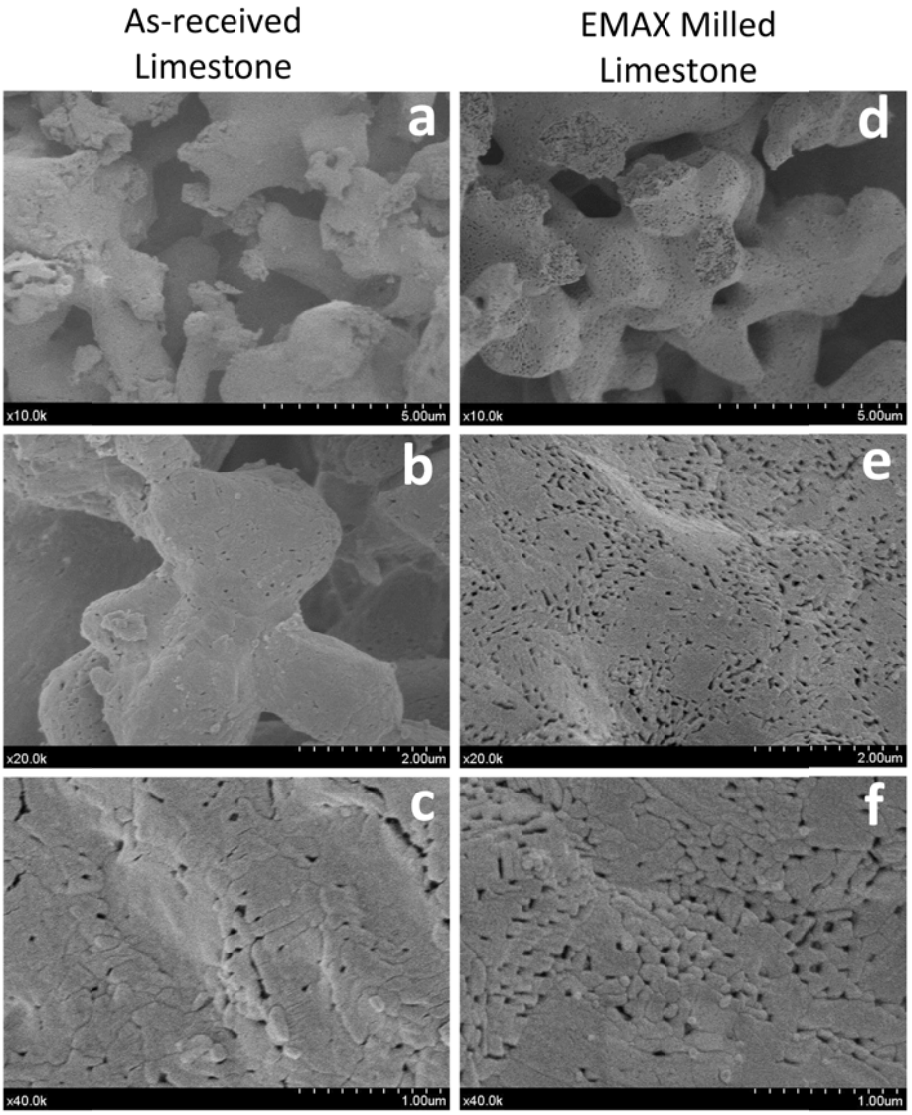
As-received Limestone
EMAX Milled Limestone
a
d
x10.0k
5.00um
x10.0k
5.00um
b
e
x20.0k
2.00um
x20.0k
2.00um
c
f
x40.0k
1.00um
x40.0k
1.00um

Figure 8

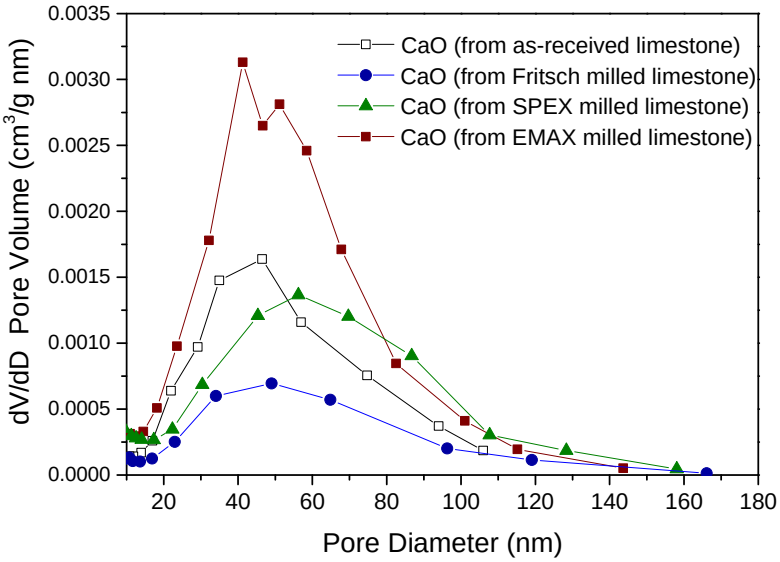
0.0035
0.0030
0.0025
0.0020
0.0015
0.0010
0.0005
0.0000
dV/dD Pore Volume (cm3/g nm)
20
40
60
80
100
120
140
160
180
Pore Diameter (nm)
CaO (from as-received limestone)
CaO (from Fritsch milled limestone)
CaO (from SPEX milled limestone)
CaO (from EMAX milled limestone)

Figure 9

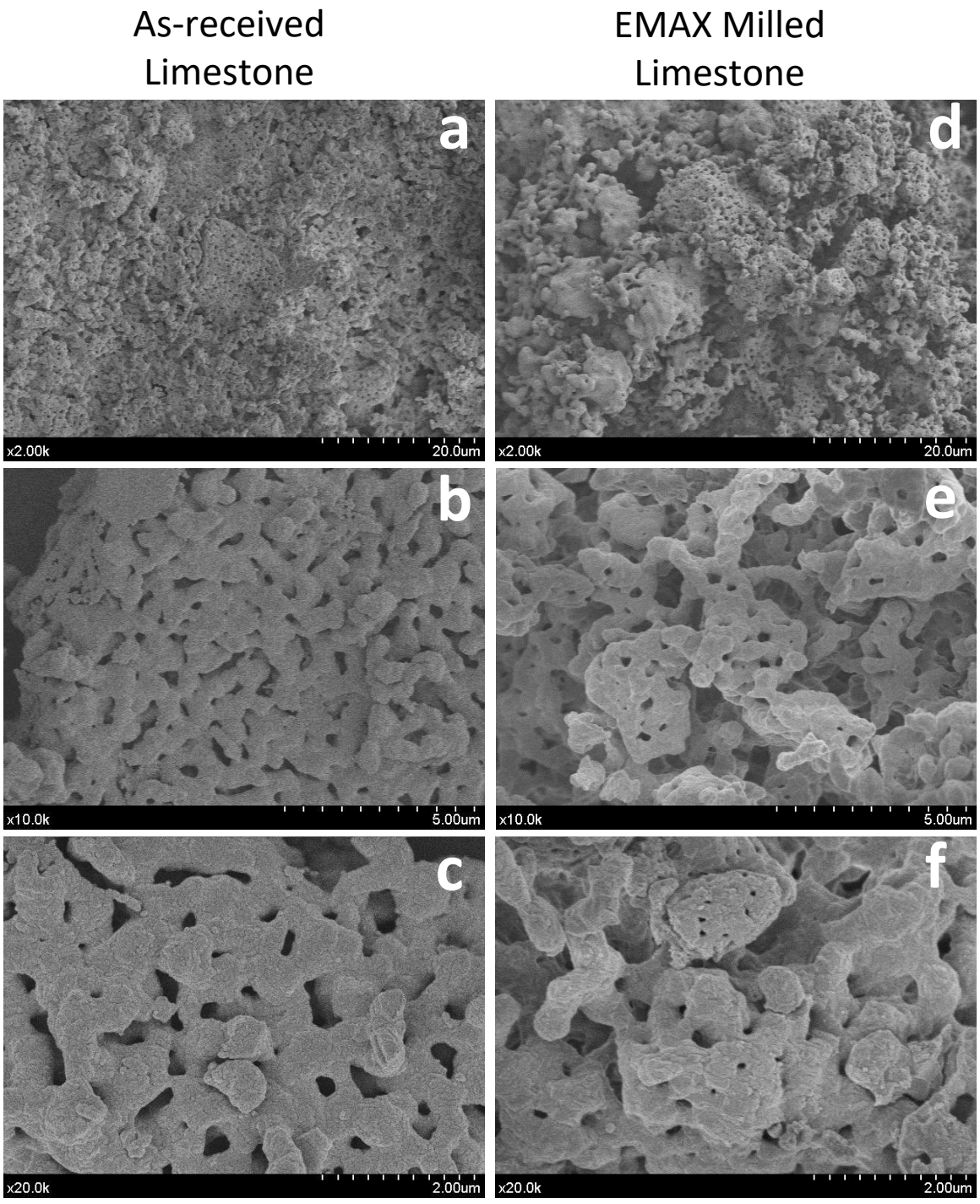
As-received Limestone
EMAX Milled Limestone
a
d
x2.00k
20.0um
x2.00k
20.0um
b
e
x10.0k
5.00um
x10.0k
5.00um
c
f
x20.0k
2.00um
x20.0k
2.00um

Figure 10

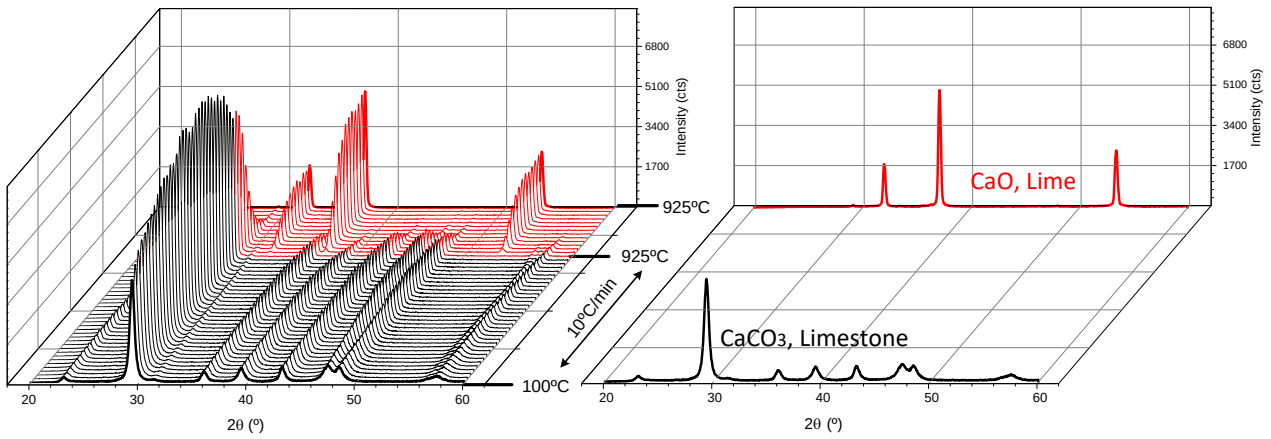
6800
5100
3400
1700
Intensity (cts)
925ºC
925ºC
10ºC/min
100ºC
20
30
40
50
60
2θ (º)
CaO, Lime
CaCO3, Limestone

Figure 11

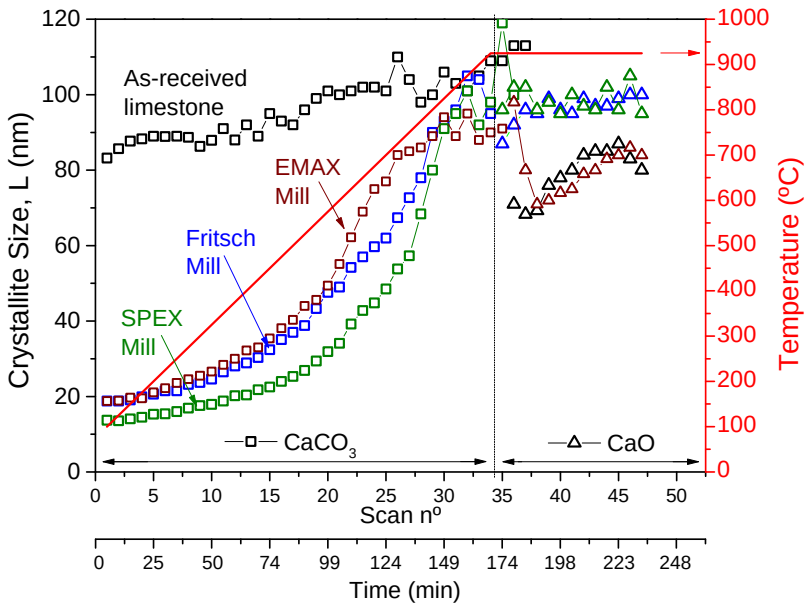
Crystallite Size, L (nm)
Temperature (°C)
As-received
limestone
EMAX
Mill
Fritsch
Mill
SPEX
Mill
CaCO3
CaO
Scan nº
Time (min)
0
5
10
15
20
25
30
35
40
45
50
0
25
50
74
99
124
149
174
198
223
248
0
20
40
60
80
100
120
0
100
200
300
400
500
600
700
800
900
1000

Figure A1 (Appendix)